Quantum Hall Effect on Top and Bottom Surface States of Topological Insulator $(Bi_{1-x}Sb_x)_2Te_3$ Films

R. Yoshimi[1*], A. Tsukazaki[2,3], Y. Kozuka[1], J. Falson[1], K. S. Takahashi[4], J. G. Checkelsky[1+],

N. Nagaosa[1,4], M. Kawasaki[1,4] and Y. Tokura[1,4]

[1] *Department of Applied Physics and Quantum-Phase Electronics Center (QPEC),*

University of Tokyo, Tokyo 113-8656, Japan

[2] *Institute for Materials Research, Tohoku University, Sendai 980-8577, Japan*

[3] *PRESTO, Japan Science and Technology Agency (JST), Chiyoda-ku, Tokyo 102-0075,*

Japan

[4] *RIKEN Center for Emergent Matter Science (CEMS), Wako 351-0198, Japan.*

* Corresponding author: yoshimi@cmr.t.u-tokyo.ac.jp

+ present address: *Massachusetts Institute of Technology, Cambridge, Massachusetts*

02139, USA

Abstract

The three-dimensional topological insulator is a novel state of matter characterized by two-dimensional metallic Dirac states on its surface. To verify the topological nature of the surface states, Bi-based chalcogenides such as Bi_2Se_3, Bi_2Te_3, Sb_2Te_3 and their combined/mixed compounds have been intensively studied. Here, we report the realization of the Quantum Hall effect on the surface Dirac states in $(Bi_{1-x}Sb_x)_2Te_3$ films. With electrostatic gate-tuning of the Fermi level in the bulk band gap under magnetic fields, the quantum Hall states with filling factor ±1 are resolved. Furthermore, the appearance of a quantum Hall plateau at filling factor zero reflects a pseudo-spin Hall insulator state when the Fermi level is tuned in between the energy levels of the non-degenerate top and bottom surface Dirac points. The observation of the Quantum Hall effect in three-dimensional topological insulator films may pave a way toward topological-insulator-based electronics.

Introduction

Quantum transport in Dirac electron systems has been attracting much attention for the half-integer quantum Hall effect (QHE), as typically observed in graphene[1, 2]. A single Dirac fermion under an magnetic field is known to show the quantized Hall effect with the Hall conductance $\sigma_{xy} = (n + 1/2)e^2/h$ with n being an integer, e the elemental charge and h Planck constant. This 1/2 is the characteristic of the Dirac fermion compared with the usual massive electrons. In graphene with such a Dirac electron, however, there is four-fold degeneracy due to the spin and valley degrees of freedom, and hence the quantized Hall conductance shows up experimentally as $\sigma_{xy} = 4(n + 1/2)e^2/h$. The recently discovered topological insulator (TI) possesses metallic Dirac states on the edge or surface of an insulating bulk[3-6]. With the application of a magnetic field (B) the unique features of Dirac bands may be exemplified via the formation of Landau levels (LLs). The QHE is the hallmark of dissipationless topological quantum transport originating from one-dimensional chiral edge modes driven by cyclotron motion of two-dimensional (2D) electrons. Unlike the case of graphene, the degeneracy is completely lifted in the spin-polarized Dirac state of 2D and three-dimensional (3D) TIs. The Hall conductance σ_{xy} of 3D TI is expected to be given by the sum of the two contributions from top and bottom surfaces and hence $\sigma_{xy} = (n$

+ n'+ 1)e^2/h with both n and n' being integers. When the two contributions are equivalent,

i.e. $n = n$', only the odd integer QHE is expected. For such 3D TI films the top and bottom

surfaces support surface states with opposite spin-momentum locked modes when top and

bottom surfaces are regarded as two independent systems. Such a helicity degree of

freedom in real space can be viewed as the pseudo-spin variable and is hence expected to

yield a new quantum state via tuning of surface magnetism and/or Fermi level (E_F) that is

applicable to quantum computation functions[7-9]. Although intensive research has been

carried out for bulk crystals, thin films, and field-effect devices[10-17], parasitic bulk

conduction and/or disorder in the devices continues to hamper efforts to resolve quantum

transport characteristics of the Dirac states on chalcogenide 3D TIs surfaces. The most

venerable example of the QHE with least bulk conduction has been achieved in 70 nm

strained HgTe film[18]. Compared to the HgTe system, 3D-TIs of Bi-chalcogenides such as

Bi_2Se_2Te and $(Bi_{1-x}Sb_x)_2Te_3$ have a good potential for exploring the Dirac surface states

with wide controllability of transport parameters (resistivity, carrier type and density) and

band parameters (energy gap, position of Dirac point and Fermi velocity) by changing the

compositions[19, 20].

In the following, we report on the QHE in the field-effect transistor based on 3D TI thin

films of $(Bi_{1-x}Sb_x)_2Te_3$ ($x = 0.84$ and 0.88). With electrostatic gate-tuning of the Fermi level

in the bulk band gap under magnetic fields, quantized Hall plateaus ($\sigma_{xy} = \pm e^2/h$) at the

filling factor $\nu = \pm 1$ are resolved, pointing to the formation of chiral edge modes at

top/bottom surface Dirac states. In addition, the emergence of a $\sigma_{xy} = 0$ state around the

charge neutral point (CNP) reflects a pseudo-spin Hall insulator state when the location of

Fermi level is between the non-degenerate top and bottom surface Dirac points.

Results

Transport properties with electrostatic gate-tuning   We grew 3D TI thin films of

$(Bi_{1-x}Sb_x)_2Te_3$ ($x = 0.84$ and 0.88; both 8 nm thick) using molecular beam epitaxy[19] and

insulating InP (111) substrates. The E_F of as-grown film was tuned near to the bulk band

edge by precisely controlling the Bi/Sb composition ratio in the film[19, 20]. Films were then

fabricated into photolithography-defined gated Hall-bar devices to allow electrostatic

tuning of E_F. A cross-sectional schematic of the device structure and the top-view image are

shown in Figs. 1a and 1b, respectively. The device consists of Hall bar defined by Ar

ion-milling, and an atomic-layer-deposited AlO_x insulator isolates Ti/Au top gate with

electron-beam evaporated Ti/Au electrodes (see Methods). The magnetotransport

measurements were carried out in a dilution refrigerator by low-frequency (3 Hz) lock-in technique with low excitation current of 1 nA to suppress heating (see Supplementary Note 1).

First, device operation was examined at $B = 0$ T. Figure 1c shows the electric field effect controlled conductivity σ_{xx} of the $x = 0.84$ film as a function of top gate voltage V_G with changing temperature. The minimum conductivity of roughly $2e^2/h$ is observed at $V_G = -1.7$ V. On both sides of this minimum, σ_{xx} shows a linear but asymmetric increase with increasing or decreasing V_G. The weak temperature dependence of longitudinal conductivity σ_{xx} for a wide range of V_G is characteristic of the gapless nature of Dirac states under finite disorder[21]. Thus we ascribe the conductivity of this TI film below 1 K to the Dirac surface states with a small contribution from bulk conduction. To verify the ambipolar nature of the device, the longitudinal and transverse resistance R_{xx} and R_{yx} as a function of V_G at $B = 3$ T were measured (Fig. 1d). As expected, this results in a sign change of R_{yx} at a certain V_G which we hereafter define as the gate voltage corresponding to E_F being located at the charge neutral point (CNP), V_{CNP}. This point coincides closely with the V_G at which R_{xx} reaches a maximum. At the V_{CNP}, the Hall effects from top and bottom surface states appear to cancel, resulting in $R_{yx} \sim 0$, although electron-rich and hole-rich

puddles are thought to still exist, as in the case of graphene[22]. To capture the essence of the observed phenomena, we hereafter take the working hypothesis that E_F shifts equally on top and bottom states which in turn retain the difference in energy position. The inverse of Hall coefficient $1/R_H$ is shown in Fig. 1e, which would be proportional to 2D charge carrier density $n_{2D} = 1/(eR_H)$, in the simplest case. Asymmetric behavior of $1/R_H$ between positive and negative V_G regions with respect to V_{CNP} is in accord with the asymmetric σ_{xx} behavior at zero magnetic field as shown in Fig. 1c. The more efficient increase in σ_{xx} with electron accumulation (positive V_G) is often observed in ambipolar TI transistors[13-17] and may be related to the difference in v_F (Fermi velocity) above and below the Dirac point[19]. In addition, the proximity of the Dirac point to the valence band edge needs to be taken into account for the present thin film system; in most of the negative region of $V_G - V_{CNP}$, E_F must go inside the valence band in which doped holes appears to be fully localized at low temperatures below 1 K, as argued later.

Observation of quantum Hall states With applying higher magnetic field of $B = 14$ T, clear signatures of QHE are revealed in the temperature dependence of R_{xx} and R_{yx}, as shown in Figs. 2a-d for the $x = 0.84$ film and in Figs. 2e-h for the $x = 0.88$ film. We first focus on the results of the $x = 0.84$ film. R_{xx} increases steeply with lowering the temperature

7

for V_G corresponding to the CNP, while decreases rapidly toward zero in the both sides at higher and lower V_G. Concomitantly to the decrease in R_{xx}, R_{yx} reaches the values of quantum resistance $\pm h/e^2 = \pm 25.8$ kΩ and forms plateaus in V_G at $T = 40$ mK. This correspondence between the rapidly declining R_{xx} value and the quantized R_{yx} plateaus at $\pm h/e^2$ are distinct evidence for QHE at Landau filling factor $\nu = \pm 1$, respectively, as schematically shown in Fig. 2i (magnetic field dependence is shown in Supplementary Fig. 2). The LL splitting energy of Dirac dispersion (E_n) is given by $E_n = \mathrm{sgn}(n)\sqrt{2\,|n|\,\hbar v_F^2 eB}$, where n is the LL index.

Using the data of R_{xx} and R_{yx}, σ_{xy} and σ_{xx} as functions of $V_G - V_{CNP}$ for the $x = 0.84$ film are plotted in Figs. 2c and 2d. Again, the Hall plateaus at $\sigma_{xy} = \pm e^2/h$ as well as minima of σ_{xx} approaching zero (black triangles) are observed and are indicative of the QHE with $\nu = \pm 1$. In this plot, however, two additional features are to be noted. The first is an unexpectedly wide σ_{xy} plateau and thermally activated behavior of σ_{xx} for the $\nu = +1$ ($\sigma_{xy} = e^2/h$) state in the corresponding $V_G - V_{CNP}$ (negative) region. As already noted in the V_G asymmetric change of σ_{xx} (Fig. 1c) in the negative region of $V_G - V_{CNP}$, *i.e.* hole-doping, E_F readily reaches the valence band top. The energy position of Dirac point of the $x = 0.84$ film lies by at most 30 meV above the valence band top, while the LL splitting between $n =$

8

0 and $n = -1$ levels amounts to 70 meV at 14 T, according to resonant tunneling spectroscopy on similarly grown thin films of $(Bi_{1-x}Sb_x)_2Te_3$ (Ref. 19). From the consideration of the Fermi velocity of Dirac cone, the $V_G - V_{CNP}$ value at which the E_F reaches the valence band top is estimated to be around -1.5 V or an even a smaller absolute value. Therefore, in the $V_G - V_{CNP}$ region where the quantum Hall plateau or its precursor is observed, the E_F locating between $n = 0$ and $n = -1$ LLs of the surface state is close to or already buried in the valence band, as schematically shown in Fig. 2i. While the doped but localized holes in the valence band may hardly contribute to transport, *i.e.* σ_{xy}(bulk) $<< \sigma_{xy}$ (surface), the relative E_F shift with negatively sweeping $V_G - V_{CNP}$ becomes much slower as compared with the positive sweep case owing to the dominant density of states of the valence band. This explains a wider plateau region for $v = +1$ in the hole-doping side, contrary to the normal behavior of electron accumulation side, $v = -1$.

The second notable feature in Fig. 2c is the emergence of the $v = 0$ state around $V_G = V_{CNP}$, as seen in the step of σ_{xy} and (finite) minimum in σ_{xx} as functions of $V_G - V_{CNP}$. This state is more clearly resolved in the $x = 0.88$ film, as shown in Figs. 2e-h, on which we focus hereafter. In a similar manner to the $x = 0.84$ film, the $x = 0.88$ film also shows with lowering temperature divergent behavior of R_{xx} around $V_G = V_{CNP}$, while approaching zero

9

around $V_G - V_{CNP} = -1.5$ V. The similar divergent (at $V_G = V_{CNP}$) and vanishing (at $V_G -$

$V_{CNP} = -1.5$ V) behaviors of R_{xx} are observed also with increasing B at 40 mK (see

Supplementary Fig. 3). The R_{yx} reaches 25.8 kΩ around $V_G - V_{CNP} = -1.5$ V forming the $v =$

+1 quantum Hall state, while in the electron doping regime R_{yx} reaches -20 kΩ, short of the

quantized value. The failure to form the fully quantized $v = -1$ state is perhaps related to

the disorder of the surface Dirac state which is induced by the compositional/structural

disorder of the as-grown film and cannot be overcome by gate tuning.

Nevertheless, the $v = 0$ feature is clearly resolved for the $x = 0.88$ film, as shown in the

V_G dependence of σ_{xy} (Fig. 2g) calculated from R_{xx} and R_{yx}. In addition to the $\sigma_{xy} = e^2/h$ (v

$= +1$) plateau, a plateau at $\sigma_{xy} = 0$ appears at around $V_G = V_{CNP}$. The plateau broadening

occurs via centering at $\sigma_{xy} = 0.5\ e^2/h$ as the isosbestic point with elevating temperature. In

accordance with the plateaus in σ_{xy}, σ_{xx} takes a minima at $v = +1$ and 0, as shown in Fig. 2h.

Here, we can consider the contribution of the both top and bottom surface Dirac states to

this quantization of σ_{xy}, as schematically shown in Fig. 2j. At the $v = +1$ ($v = -1$) state, the

both top and bottom surfaces are accumulated by holes (electrons) with E_F being located

between $n = 0$ and $n = -1$ ($n = +1$) LLs, giving rise to the chiral edge channel. In contrast,

we assign the $v = 0$ state to the gapping of the chiral edge channel as the cancelation of the

10

contributions to σ_{xy} from the top and bottom surface states with $\nu = \pm 1/2$, when E_F locates

in between the energy levels of the top and bottom surface Dirac points ($n = 0$ levels), as

shown in Fig. 2j. This $\nu = 0$ state can hence be viewed as a *pseudo-spin Hall insulator*, if

we consider the top and bottom degree of freedom as the pseudo-spin variable. Such an

observation of a zero conductance plateau has been reported also in disordered graphene

under very high magnetic field[23-26] and analyzed theoretically[27], as well as in the 2D TIs,

the quantum wells of HgTe[28] and InAs/GaSb[29]. From the analyses shown in the following,

we propose here that the major origin for the presence of $\sigma_{xy} = 0$ is more like the energy

difference of the top/bottom Dirac points rather than other effects such as electron-hole

puddles in composition inhomogeneity.

Discussion

To further discuss the characteristics of these QH states, we investigate the B dependence of

σ_{xy} (Figs. 3a and b). The analysis of the plateau width against V_G determines the phase

diagram as shown in Figs. 3c and d. The plateau edges are determined from the second

derivative of σ_{xy} with respective to V_G (see Supplementary Fig. 4), while the plateau

transition points between $\nu = 0$ and $\nu = \pm 1$ are defined here by $\sigma_{xy} = \pm\ e^2/2h$. The

plateau shrinks with decreasing B for the $\nu = -1$ state of the $x = 0.84$ film (Fig. 3a).

However, the $\nu = +1$ state for the both films appears to be rather robust with reducing V_G

(doping more holes), since E_F positions already below the top of the valence band, perhaps

for $V_G - V_{CNP} < -1.5$ V. On the other hand, the $\nu = 0$ plateau is only weakly dependent on B,

although the plateau width is wider for $x = 0.88$ than for $x = 0.84$. The observation of $\nu = 0$

requires the condition that the Fermi level is located in between the energy levels of the top

and bottom surface Dirac points (Fig. 2j). From the Hall data in the relatively high positive

$V_G - V_{CNP}$ region (electron-doping) shown in Fig. 1e, we can know the relation between the

sum of the top and bottom Dirac electron density versus $V_G - V_{CNP}$. Then, with the values

of the $\nu = 0$ plateau width between the $\sigma_{xy} = \pm 0.5\ e^2/h$ points ($\delta V_G \sim 0.9$ V and 1.4 V; see

Figs. 3c and d) and the Fermi velocity ($v_F \sim 5\times 10^5$ ms^{-1})[19], we can estimate the energy

difference (δE_{DP}) between the Dirac points at the top and bottom surface states to be ~ 50

meV and ~ 70 meV for the $x = 0.84$ and $x = 0.88$ film, respectively (see Supplementary

Note 5). These values should be compared with a much larger band gap energy (~ 250

meV). The energy difference δE_{DP} is, however, considerably larger than a Zeeman shift (~ 9

meV at 14 T)[19], which rationalizes the above analysis with ignoring the Zeeman shift of the

$n = 0$ LL. While the reason why the two films ($x = 0.84$ and 0.88) show such a difference in

12

δE_{DP} is not clear at the moment, we speculate that the monolayer buffer layer of Sb_2Te_3 ($x =$ 1.0) used for the growth of the $x = 0.88$ film (see Methods) may cause the considerably higher energy position of the Dirac point at the bottom surface. Incidentally, for the region of $|V_G - V_{CNP}| < \delta V_G/2$, electron accumulation at the top surface and hole accumulation at the bottom surface should coexist. This may naturally explain the observed (Fig. 1e and see also Supplementary Fig. 5) deviation from the linear relationship between $1/R_H$ and $V_G - V_{CNP}$ as well as the extrema of $1/R_H$ observed at around $\pm \delta V_G/2$.

Figure 4 summarizes the flow of conductivity tensor (σ_{xy}, σ_{xx}) plotted with the two experimental subparameters (T and V_G) at 14 T. With decreasing T, the flow in (σ_{xy}, σ_{xx}) tends to converge toward either of (σ_{xy}, σ_{xx}) = ($-e^2/h$, 0), (0, 0) or (e^2/h, 0) at high magnetic field (e.g. 14 T), which corresponds to $\nu = -1$, 0 and $+1$ QH state, respectively. Incipient convergence to $\nu = 0$ is discerned for the $x = 0.84$ film, while the $\nu = -1$ state is not discernible for the $x = 0.88$ film. Among these three QH states, the unstable fixed point appears to lie on the line of $\sigma_{xy} = \pm 0.5\ e^2/h$ (approximately with the critical σ_{xx} value of $\sim$ 0.5 e^2/h) which corresponds to the crossing of E_F at the $n = 0$ LL (or Dirac point) of the bottom and top surface state (see Fig. 2j), respectively[30].

In conclusion, we have successfully observed the QHE at $\nu = \pm 1$ and 0 states in

three-dimensional TI thin films of $(Bi_{1-x}Sb_x)_2Te_3$ ($x = 0.84$ and 0.88). Due to a considerable difference of the Dirac point (or $n = 0$ LL) energies of the top and bottom surfaces of the thin film, the $\nu = 0$ state observed at $\sigma_{xy} = 0$ is interpreted as a pseudo-spin Hall insulator with the top/bottom degree of freedom as the pseudo-spin. Further studies on non-local transport in mesoscopic structures will open the door to dissipationless topological-edge electronics based on the 3D topological insulators.

Methods

MBE film growth   Thin films of $(Bi_{1-x}Sb_x)_2Te_3$ ($x = 0.84$ and 0.88) were fabricated by molecular beam epitaxy (MBE) on semi-insulating InP (111) substrate. The Bi/Sb composition ratio was calibrated by the beam equivalent pressure of Bi and Sb, namely 8×10^{-7} Pa and 4.2×10^{-6} Pa for $x = 0.84$ and 6×10^{-7} Pa and 4.4×10^{-6} Pa for $x = 0.88$. The Te flux was over-supplied with the Te / (Bi + Sb) ratio kept at about 20. The substrate temperature was 200°C and the growth rate was about 0.2 nm per minute. Fabrication procedures for the $x = 0.84$ and 0.88 films are slightly different at the initial growth on InP surfaces. We grew the 0.84 film with supplying Te and (Bi + Sb) from the initial stage. For the $x = 0.88$ film, we started with supplying Te and Sb for a monolayer growth of Sb_2Te_3 buffer layer followed by Bi shutter opening. This difference may be an origin of the larger energy gap δE_{DP} of the Dirac points between the top and bottom surfaces (Fig. 2j) for the $x = 0.88$ film. After the epitaxial growth of 8nm-thick thin films, those were annealed *in-situ* at 380°C to make the surface smoother.

Device fabrication AlO_x capping layer was deposited at room temperature with an atomic layer deposition system immediately after the discharge of the samples from MBE. This process turned out to be effective to protect the surface from the degradation. The

15

device structure was defined by subsequent photolithography and Ar ion-milling processes. Ohmic-contact electrodes and top gate electrode were Ti/Au deposited with an e-beam evaporator. Here, ion-milling was performed under 45 degree tilt condition on a rotating stage, resulting in the ramped side edge as schematically shown in Fig. 1a. This ensured the electrical contact to the top and bottom of the film.

References

1. Novoselov, K. S., *et al.* Two-dimensional gas of massless Dirac fermions in graphene. *Nature* **438**, 197-200 (2005).

2. Zhang, Y., Tan, Y. -W., Stormer, H. L. & Kim, P. Experimental observation of the quantum Hall effect and Berry's phase in graphene. *Nature* **438**, 201-204 (2005).

3. Hasan, M. Z. & Kane, C. L. Colloquium: Topological insulators. *Rev. Mod. Phys.* **82**, 3045 (2010).

4. Kane, C. L. & Mele, E. J. Z_2 Topological Order and the Quantum Spin Hall Effect. *Phys. Rev. Lett.* **95**, 146802 (2005).

5. Fu, L., Kane, C. L. & Mele, E. J. Topological insulators in three dimensions. *Phys. Rev. Lett.* **98**, 106803 (2007).

6. Hsieh, D. *et al.* A tunable topological insulator in the spin helical Dirac transport regime. *Nature* **460**, 1101-1105 (2009).

7. Yu., R., *et al*. Quantized Anomalous Hall Effect in Magnetic Topological Insulators. *Science* **329**, 61-64 (2010).

8. Chang, C. –Z., *et al*. Experimental Observation of the Quantum Anomalous Hall Effect in a Magnetic Topological Insulator. *Science* **340**, 167-170 (2013).

9. Wang, J., Lian, B., Zhang, H. & Zhang, S. –C. Anomalous Edge Transport in the Quantum Anomalous Hall State. *Phys. Rev. Lett.* **111**, 086803 (2013).

10. Analytis, J. G., *et al.* Two-dimensional surface state in the quantum limit of a topological insulator *Nature Phys.* **6**, 960-964 (2010).

11. Qu, D. X., Hor, Y. S., Xiong, J., Cava, R. J. & Ong, N. P. Quantum Oscillations and Hall Anomaly of Surface States in the Topological Insulator Bi_2Te_3. *Science* **329**, 821-824 (2010).

12. Taskin, A. A., Ren, Z., Sasaki, S., Segawa, K. & Ando, Y. Observation of Dirac Holes and Electrons in a Topological Insulator. *Phys. Rev. Lett.* **107**, 016801 (2011).

13. Checkelsky, J. G., Hor, Y. S., Cava, R. J. & Ong, N. P. Bulk Band Gap and Surface State Conduction Observed in Voltage-Tuned Crystals of the Topological Insulator Bi_2Se_3.

Phys. Rev. Lett. **106**, 196801 (2011).

14. Steinberg, H., Laloë, J. –B., Fatemi, V., Moodera, J. S. & Jarillo-Herrero, P. Electrically tunable surface-to-bulk coherent coupling in topological insulator thin films *Phys. Rev. B* **84**, 233101 (2011).

15. Kong, D., *et al*. Ambipolar field effect in the ternary topological insulator $(Bi_xSb_{1-x})_2Te_3$ by composition tuning. *Nature Nanotech.* **6**, 705-709 (2011).

16. Kim, D., *et al*. Surface conduction of topological Dirac electrons in bulk insulating Bi_2Se_3. *Nature Phys.* **8**, 459-463 (2012).

17. Yang, F., *et al*. Top gating of epitaxial $(Bi_{1-x}Sb_x)_2Te_3$ topological insulator thin films. *Appl. Phys. Lett.* **104**, 161614 (2014).

18. Brüne, C., *et al*. Quantum Hall Effect from the Topological Surface States of Strained Bulk HgTe. *Phys. Rev. Lett.* **106**, 126803 (2011).

19. Yoshimi, R., *et al*. Dirac electron states formed at the heterointerface between a topological insulator and a conventional semiconductor. *Nature Mater.* **13**, 253-257 (2014).

20. Zhang, J., *et al*. Band structure engineering in $(Bi_{1-x}Sb_x)_2Te_3$ ternary topological insulators. *Nature Commun.* **2**, 574 (2012).

21. Bolotin, K. I., Sikes, K. J., Hone, J., Stormer, H. L. & Kim, P. Temperature-Dependent Transport in Suspended Graphene. *Phys. Rev. Lett.* **101**, 096802 (2008).

22. Martin, J., *et al*. Observation of electron-hole puddles in graphene using a scanning single-electron transistor. *Nature Phys.* **4,** 144-148 (2008).

23. Abanin, D. A., *et al*. Dissipative Quantum Hall Effect in Graphene near the Dirac Point. *Phys. Rev. Lett.* **98,** 196806 (2007).

24. Checkelsky, J. G., Li, L. & Ong, N. P. Zero-Energy State in Graphene in a High Magnetic Field. *Phys. Rev. Lett.* **100,** 206801 (2008).

25. Giesbers, A. J. M., *et al*. Gap opening in the zeroth Landau level of graphene. *Phys. Rev. B* **80,** 201403(R) (2009).

26. Zhao, Y., C-Zimansky, P., Ghahari, F. & Kim, P. Magnetoresistance Measurement of Graphene at the Charge Neutrality Point. *Phys. Rev.Lett*. **108**, 106804 (2012).

27. Das Sarma, S. & Yang, K. The enigma of the $\nu = 0$ quantum Hall effect in graphene. *Solid State Commun*. **149**, 1502-1506 (2009).

28. Büttner, B., *et al*. Single valley Dirac fermions in zero-gap HgTe quantum wells. *Nature Phys.* **7**, 418-422 (2011).

29. Nichele, F., *et al*. Insulating State and Giant Nonlocal Response in an InAs/GaSb

Quantum Well in the Quantum Hall Regime. *Phys. Rev. Lett.* **112,** 036802 (2014).

30. Nomura, K. & Nagaosa, N. Surface-Quantized Anomalous Hall Current and the Magnetoelectric Effect in Magnetically Disordered Topological Insulators. *Phys. Rev. Lett.* **106**, 166802 (2011).

Acknowledgements

Author contributions

R. Y. performed thin films growth and device fabrication. R. Y., Y. K. and J. F. performed the low temperature transport measurements. R. Y. analyzed the data and wrote

the manuscript with contributions from all authors. A. T., K. S. T., J. G. C., N. N., M. K. and Y. T. jointly discussed the results and guided the project. Y. T. conceived and coordinated the project.

Additional Information

Competing Financial Interests

The authors declare no competing financial interests.

Figure Legends

Figure 1 | Gating of topological insulator $(Bi_{0.16}Sb_{0.84})_2Te_3$ thin film. a, b, Cross-sectional schematic and top-view photograph of a Hall-bar device. Broken line in (**b**) indicates the position for (**a**). Scale bar, 300 μm. **c,** Top gate voltage V_G dependence of longitudinal conductivity σ_{xx} at various temperatures. **d, e,** Effective gate voltage ($V_G -$ V_{CNP}) dependence of longitudinal and transverse resistance (R_{xx} and R_{yx}) and inverse of Hall coefficient $1/R_H$ under magnetic field $B = 3$ T at temperature $T = 40$ mK. The V_G for

21

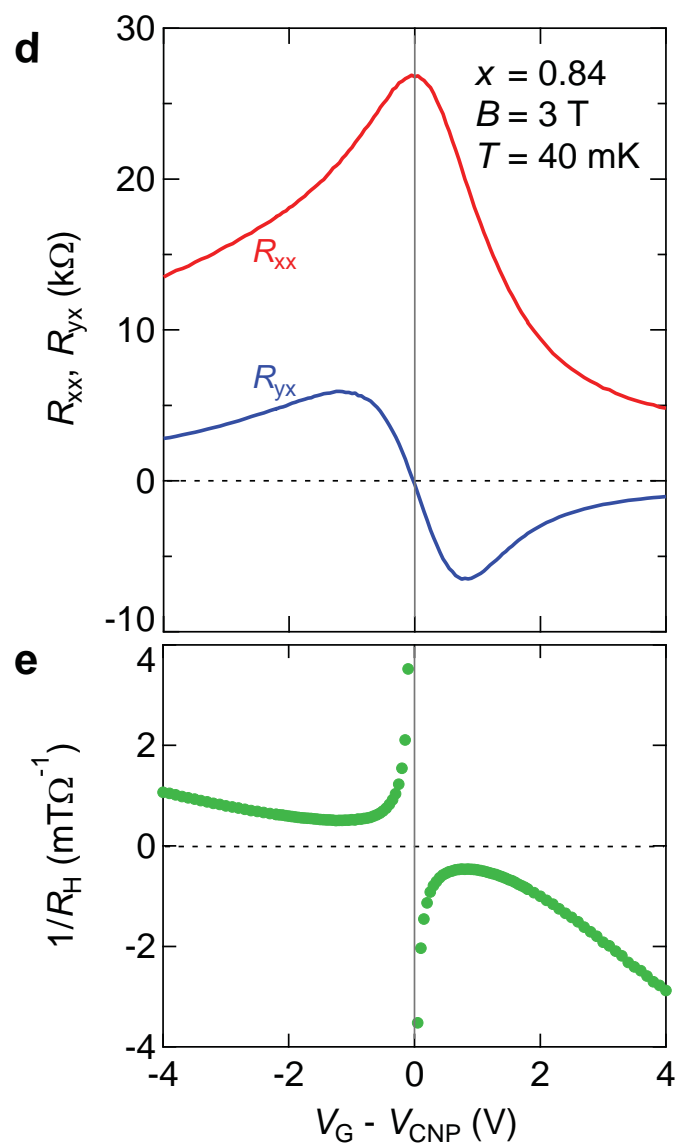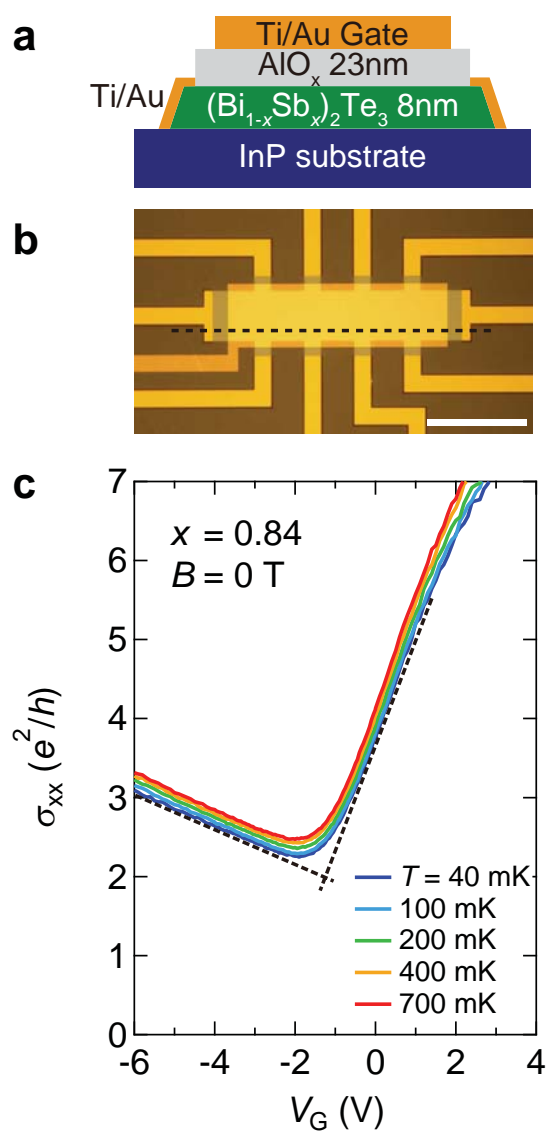the charge neutral point (CNP), V_{CNP}, is defined at the gate voltage where R_{yx} is crossing zero.

Figure 2 | Observation of the quantum Hall effect. a, b, e and f, Effective gate voltage $V_G - V_{CNP}$ dependence of R_{xx} and R_{yx} at various temperatures of $T = 40$-700 mK with application of magnetic field $B = 14$ T for the $x = 0.84$ (**a, b**) and $x = 0.88$ (**e, f**) films of $(Bi_{1-x}Sb_x)_2Te_3$. **c, d, e and h,** Effective gate voltage $V_G - V_{CNP}$ dependence of σ_{xx} and σ_{xy} at various temperatures of $T = 40$ - 700 mK with application of magnetic field $B = 14$ T for the $x = 0.84$ and $x = 0.88$ films of $(Bi_{1-x}Sb_x)_2Te_3$ as deduced from the corresponding R_{xx} and R_{yx} data. Triangles in (**d**) and (**h**) show the dips of σ_{xx}. **i,** Schematics of the Landau levels (LLs) of the surface state of $(Bi_{1-x}Sb_x)_2Te_3$ ($x = 0.8$-0.9) thin film in case of the degenerate top and bottom surface state. At a high field, *e.g.* 14 T, the $n = -1$ LL of the surface state locates below the top of the valence band. When the Fermi energy (E_F) is tuned between the LLs, the quantum Hall state with index ν emerges. **j,** Schematics of the LLs of the top and bottom surface states in case the $n = 0$ (Dirac point) energy is different between the two surfaces.

Figure 3 | Magnetic field dependence of Hall plateaus. a, b, σ_{xy} at $T = 40$ mK under various B as a function of effective gate voltage $V_G - V_{CNP}$ for the $x = 0.84$ (**a**) and $x = 0.88$

22

(**b**) films. Traces for lower magnetic fields are each vertically offset by e^2/h. Dotted lines represent the plateau transitions as defined at $\sigma_{xy} = \pm 0.5\, e^2/h$. **c, d**, Quantized σ_{xy} phase diagram for the $\nu = +1$, 0 and -1 (blue, green and red shaded, respectively) states associated with the plateau edges (filled squares) and the plateau transition point (filled circles) defined at $\sigma_{xy} = \pm 0.5\, e^2/h$ in the plane of magnetic field and $V_G - V_{CNP}$. The plateau edges are determined by the second-order V_G derivative of σ_{xy} (see Supplementary Fig. 4).

Figure 4 | Flows of σ_{xy} and σ_{xx}. $(\sigma_{xy}, \sigma_{xx})$ are displayed with the two experimental subparameters (T and V_G). Each line connecting between points represents the flow behavior of $(\sigma_{xy}, \sigma_{xx})$ with lowering temperature from 700 mK to 40 mK at the specific value of V_G at $B = 14$ T. The flows direct from upper to lower with decreasing temperature.

a
Ti/Au Gate
AlO$_x$ 23nm
Ti/Au
(Bi$_{1-x}$Sb$_x$)$_2$Te$_3$ 8nm
InP substrate

b

c
$x = 0.84$
$B = 0$ T

σ_{xx} (e^2/h)

$T = 40$ mK
100 mK
200 mK
400 mK
700 mK

V_G (V)

d
$x = 0.84$
$B = 3$ T
$T = 40$ mK

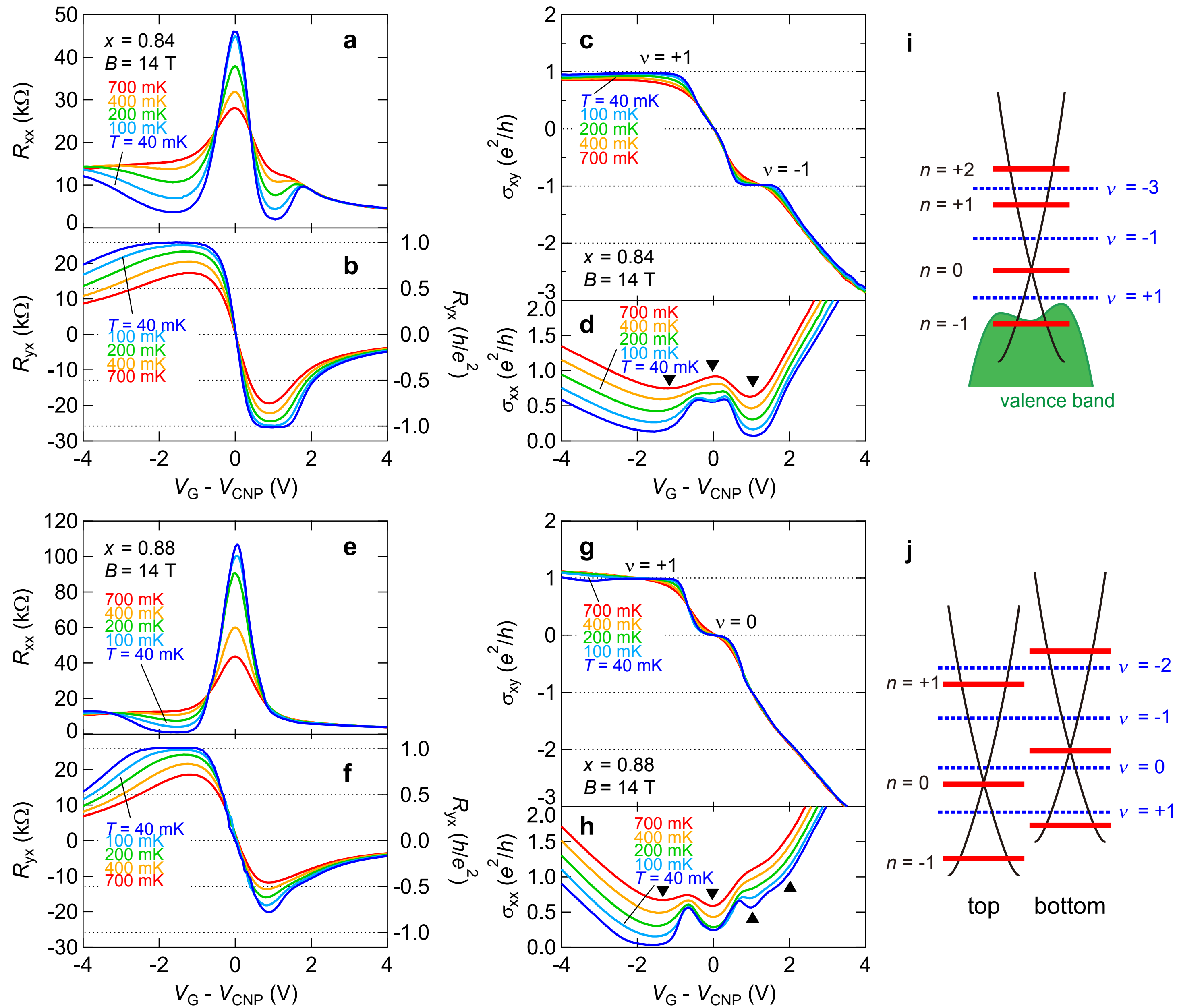R_{xx}, R_{yx} (kΩ)

R_{xx}
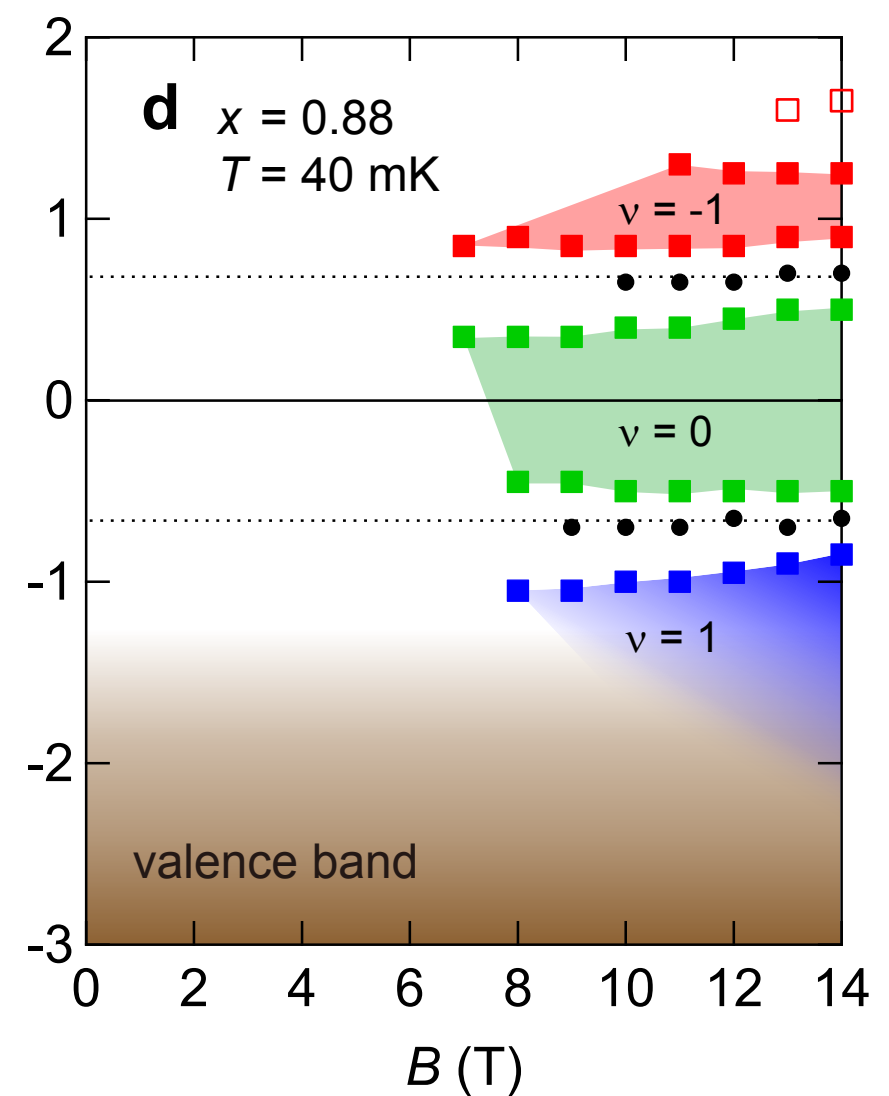
R_{yx}

e
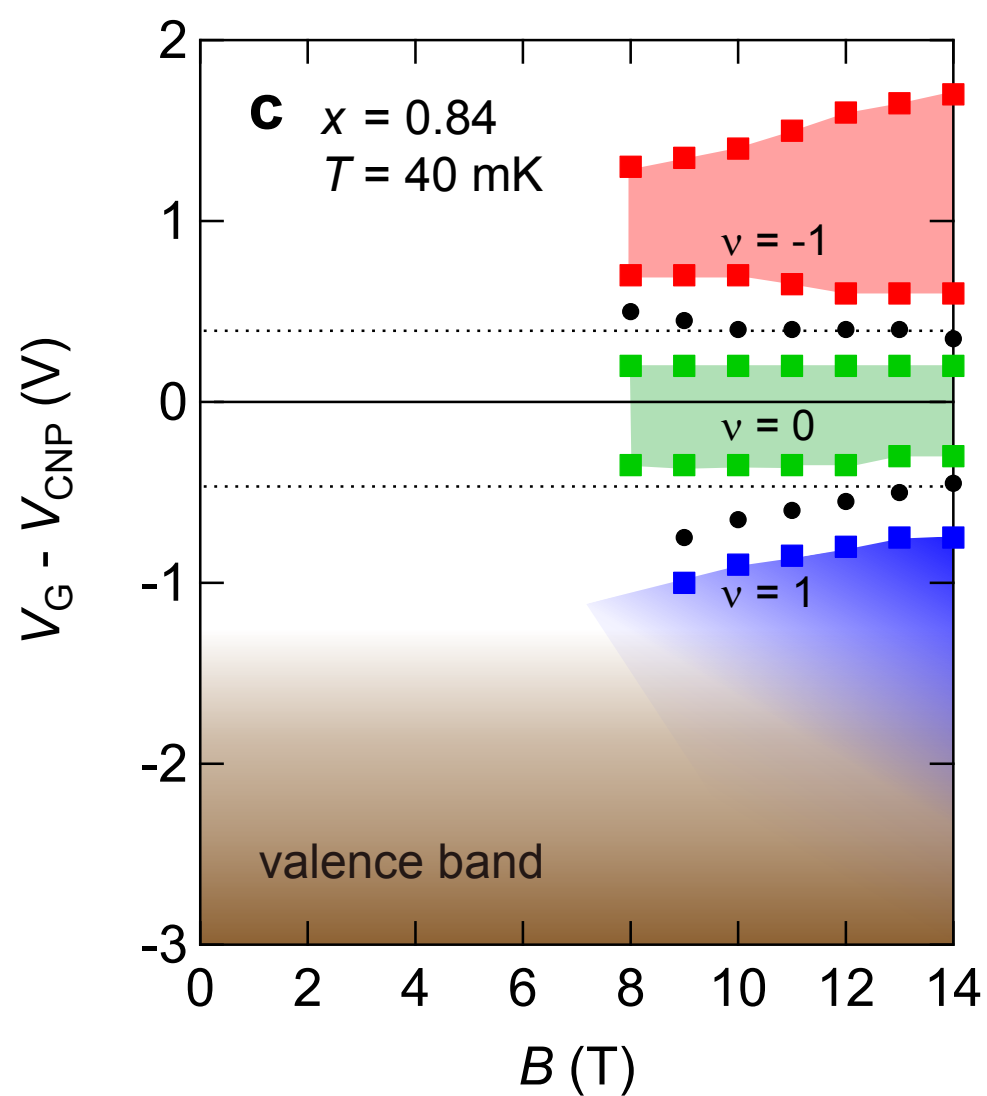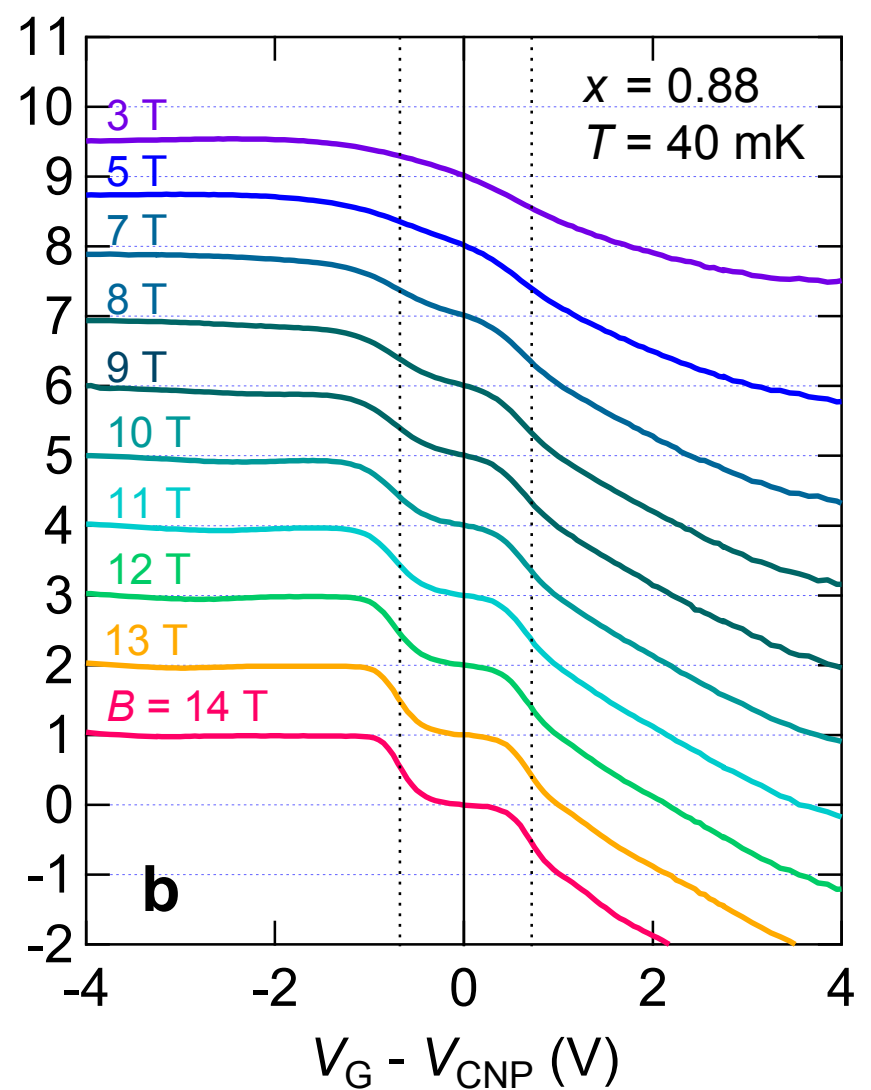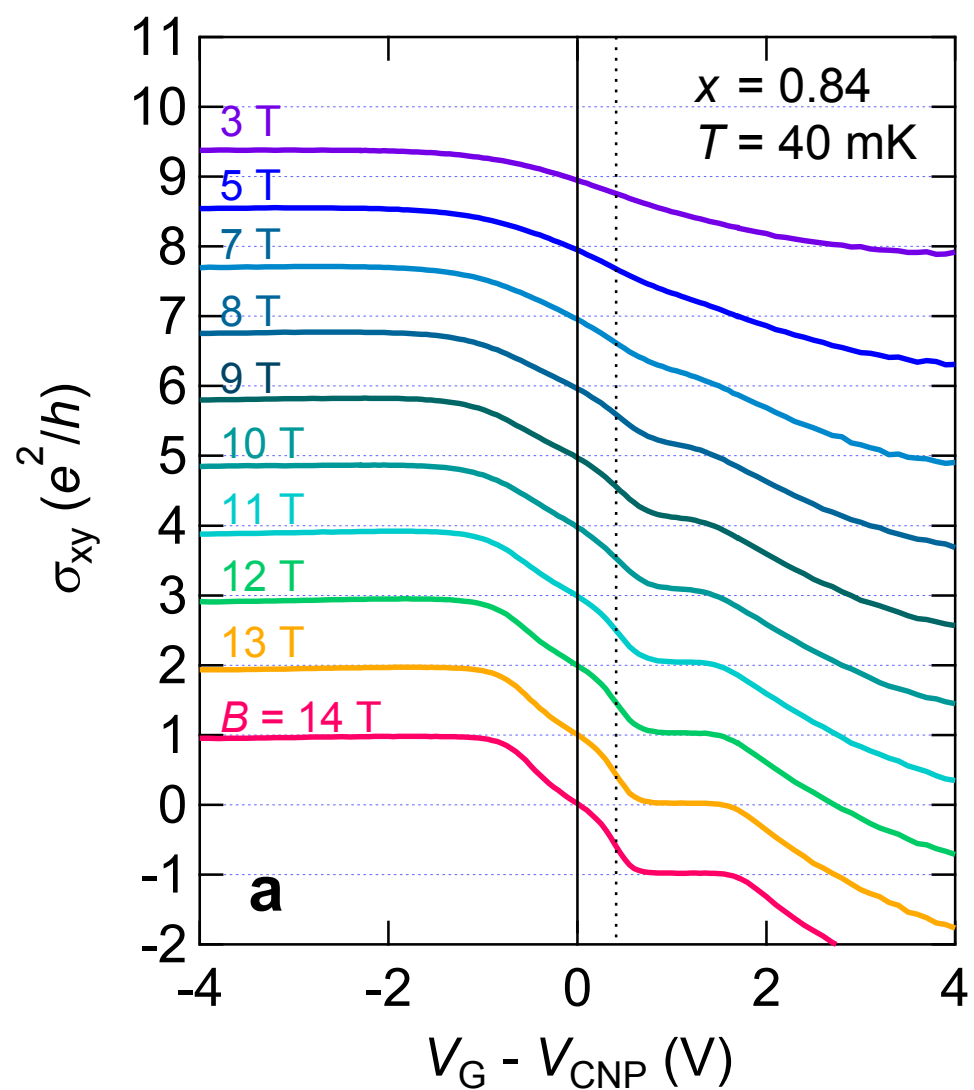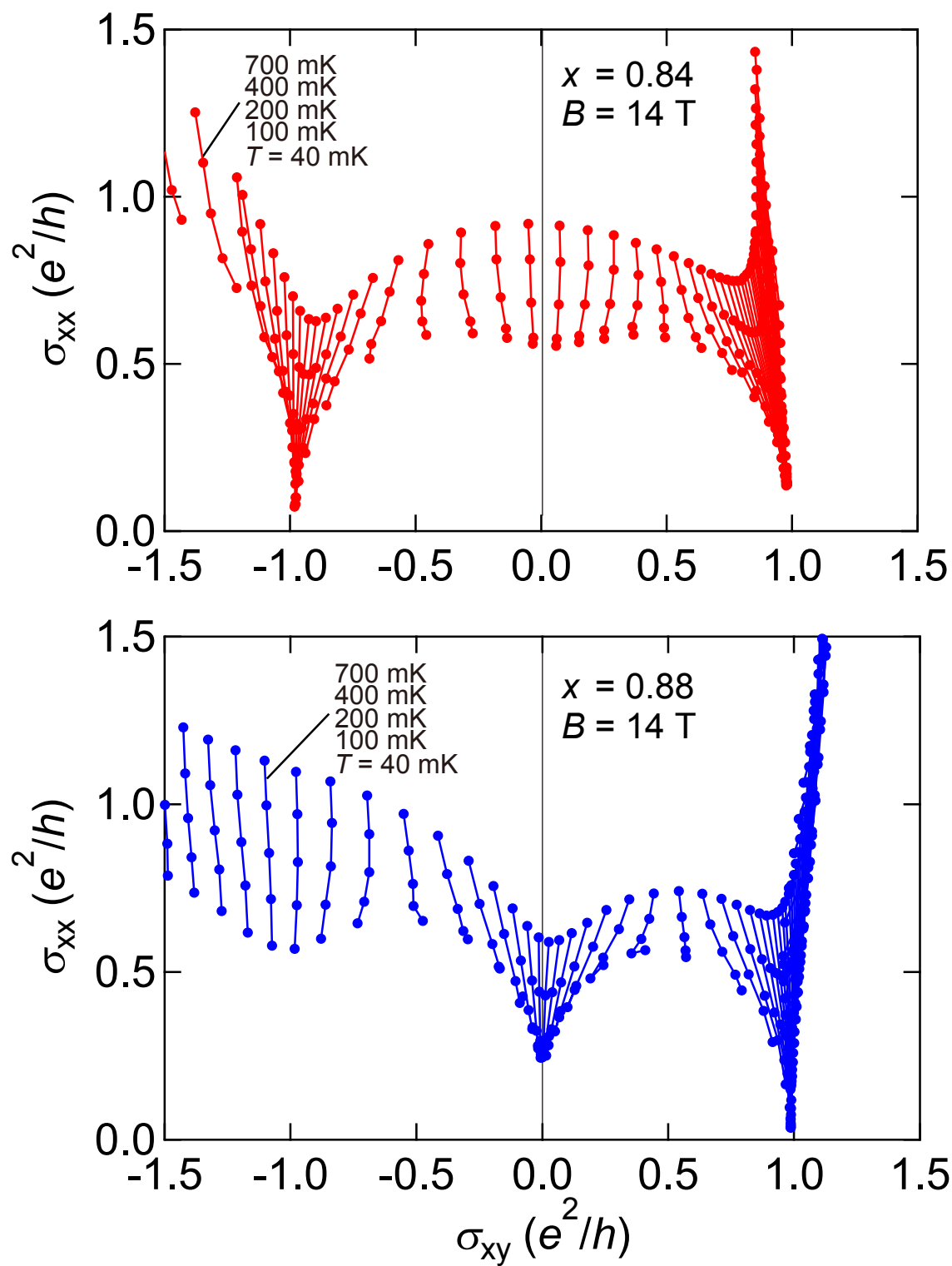$1/R_H$ (mTΩ^{-1})

$V_G - V_{CNP}$ (V)

Fig. 2 R. Yoshimi *et al.*,

Fig. 3 R. Yoshimi *et al.*,

Fig. 4 R. Yoshimi *et al.*,